

# Malicious Internet Entity Detection Using Local Graph Inference

Šimon Mandlík , Tomáš Pevný , Václav Šmídl , Lukáš Bajer 

*This document is a preprint of [1].*

**Abstract**—Detection of malicious behavior in a large network is a challenging problem for machine learning in computer security since it requires a model with high expressive power and scalable inference. Existing solutions struggle to achieve this feat—current cybersec-tailored approaches are still limited in expressivity, and methods successful in other domains do not scale well for large volumes of data rendering frequent retraining impossible. This work proposes a new perspective for learning from graph data that is modeling network entity interactions as a large heterogeneous graph. High expressivity of the method is achieved with a neural network architecture HMILnet that naturally models this type of data and provides theoretical guarantees. The scalability is achieved by pursuing local graph inference in a streamlined neighborhood subgraph, i.e., classifying individual vertices and their neighborhood as independent samples. Our experiments exhibit improvements over the state-of-the-art Probabilistic Threat Propagation (PTP) algorithm, show a threefold accuracy improvement when additional data is used, which is not possible with the PTP algorithm, and demonstrate the generalization capabilities of the method to new, previously unseen entities.

**Index Terms**—Multiple Instance Learning, Hierarchical Multiple Instance Learning, Graph Deep Learning, Computer Security, Threat Detection, Communication Networks

## I. INTRODUCTION

Detection of malicious activities in a network is a critical concern in cybersecurity. A *denylist* containing entities (second-level domains, IP addresses, emails, etc.) known for being involved in malicious activities is important either for basic blacklisting or as a source of labels for more sophisticated solutions based on machine learning. The major problem is that denylist quickly ages with time and therefore needs to be frequently updated, mostly with the help of machine learning to decrease the cost of labeling.

The most studied approach trains a classifier predicting *maliciousness* of each entity independently of others based on manually-designed features using denylist as a source of labels. For example, one can detect malicious domains with a model operating on a vector of features extracted from their URLs [2]. This *feature-based approach* is extensively researched [2]–[5], despite its weaknesses like limited expressiveness, the requirement of expert domain knowledge to

design features, and possibly deteriorating performance over time due to *concept drift* [6].

An alternative is to model interactions of entities, which is most naturally modeled as a *graph*. *Graph-based* methods in cybersecurity [7]–[9] assume that malicious activities are localized in the graph [10], [11], forming communities with sharp boundaries. Algorithms propagate maliciousness from denylisted entities to others using fixed formulas [12]–[14] with few or no hyper-parameters. This is appealing due to the seeming absence of training, but it limits the fine-tuning of the algorithm to new domains. To the best of our knowledge, these classical graph algorithms cannot utilize features on edges and vertices other than scalars.

Although the feature-based and graph-based paradigms seem complementary, one can identify several similarities. First, graph-based algorithms implicitly use features in the form of the graph (neighborhood). For example, Refs. [7], [15] estimate maliciousness of a vertex while using maliciousness of neighboring vertices and edge weights. Secondly, authors of a new graph algorithm frequently select one algorithm out of a set of candidates, which can be viewed as a form of training. In defense of graph-based algorithms, their features frequently consist only of a scalar value expressing *maliciousness* of vertices and scalar weights of edges, which makes them, to some extent, robust to changes of application domain.

We advocate a third approach (called *neighborhood-based*) that bridges the gap between the feature-based and graph-based methods [16]–[22]. Methods following this approach utilize features available for vertices and edges from a small local neighborhood. By changing the size of the neighborhood and adding or removing information in vertices and edges, neighborhood-based methods can approach the behavior of one of the two aforementioned approaches without modifications of the core algorithm.

For the purpose of this work, we use the term ‘graph inference’ for a process of estimating a scalar value of maliciousness for the entities of interest using a graph structure as the main source of knowledge.

This work presents a new neighborhood-based method for graph inference based on Hierarchical Multiple Instance Learning (HMIL) [23]–[30] tailored to the needs of the cybersecurity domain. Overall, we make the following contributions:

- We describe the new algorithm in detail and discuss its homogeneous and heterogeneous variant.
- We explain the fundamental differences to the Probabilistic Threat Propagation (PTP) algorithm [7], [15] and

Šimon Mandlík, Tomáš Pevný and Václav Šmídl are with Artificial Intelligence Center, Department of Computer Science, Czech Technical University, Prague (email: mandlsim@fel.cvut.cz; pevnymtom@fel.cvut.cz; smidlv1@fel.cvut.cz).

Lukáš Bajer is with Cisco Systems, Prague, Czech Republic (email: lubajer@cisco.com).

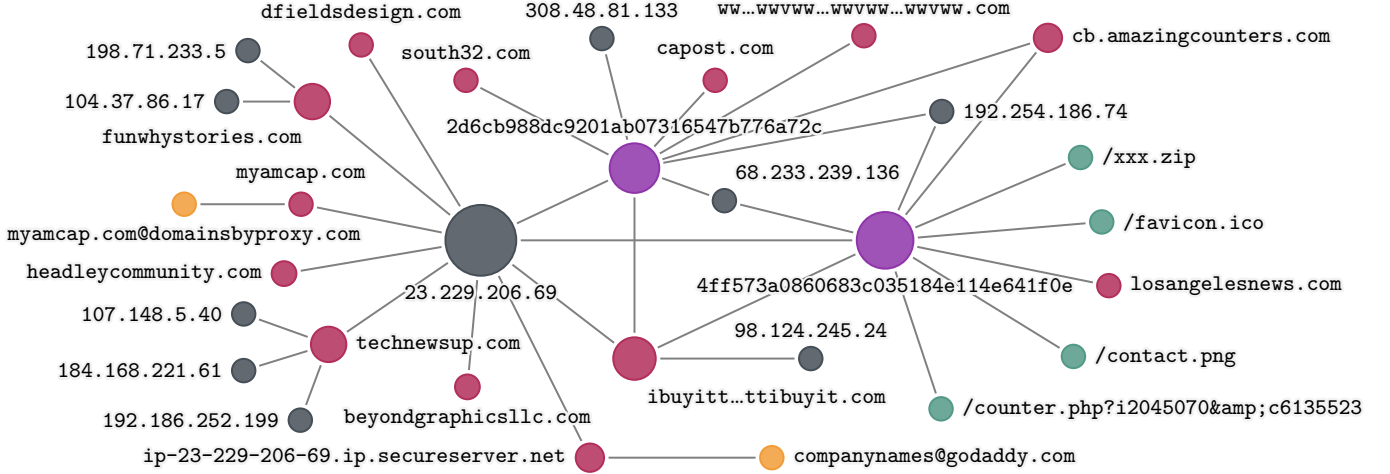


Fig. 1: An example of a network graph of binaries (represented by SHA hashes) in **purple**, second-level domains in **red**, URL paths in **green**, IP addresses in **gray**, and emails in **yellow**. Edges represent an interaction, for example, when a binary has contacted a domain hosted on an IP address or when a domain is registered with an email address. Sequences of many repeated characters in URL names were shortened using ellipsis. The example is taken from <https://www.threatcrowd.org/>, and the graph was symmetrized for demonstration purposes. Best viewed in color.

Graph neural network methods [16], [31], [32] and their heterogeneous extensions [33]–[41].

- We show how the algorithm can be used to learn from elementary network observations in the form of multiple (heterogeneous) binary relations.
- The approach is first compared to the PTP algorithm [7] in a limited setting (imposed by PTP) of modeling interactions between network clients and second-level domains.
- Then the generality of the proposed scheme is demonstrated on a task of detection of second-level domains involved in malicious activities, leveraging relations between a large number of entities in the Internet (binaries, IP addresses, TLS certificates and WHOIS registries). To the best of our knowledge, this is the first work modeling interaction of such heterogeneous entities on this scale in this domain.

The next Section II defines the problem and describes the nature of the data available on the input. Section III discusses relevant work on graphical models and reviews advances in the (Hierarchical) Multiple Instance Learning field. Section IV describes the graph processing approach based on HMIL and Section V shows an extension of the method to heterogeneous graphs, resulting in a general method for mapping the Internet using only several binary relations as input. Finally, Section VI shows the experimental comparison and Section VIII concludes the work and discusses possible future research directions. In the Supplementary material, we provide a list of important symbols, full experimental results, and dataset details.

## II. DATA AND PROBLEM DESCRIPTION

The goal of this work is to estimate the probability that any network entity (like a second-level domain, IP address, or email) is involved in malicious activity. The denylist consisting

of known malicious entities is used as a source of knowledge, however, it is almost surely incomplete. Even though the prior probability that a random non-denylisted entity is clean is high, the task is best solved as a *positive-unlabeled problem* [42], considering denylisted entities as malicious and non-denylisted entities as ‘unknown’. For evaluation purposes, we consider all non-denylisted entities benign.

We estimate the maliciousness probability by observing raw interactions in the form of binary relations involving entities in the Internet and the knowledge about their involvement in unwanted actions (which is always incomplete). Binary relations are naturally modeled as a *heterogeneous* graph, where vertices correspond to Internet entities (second-level domains, IP addresses, emails, clients, processes, etc.) and edges to interactions between them. An illustrative example is shown in Figure 1.

Since [42] lists conditions for solving positive-unlabeled problems as a supervised task, the problem can be viewed as a series of independent binary classifications of individual vertices of interest, in which case the heterogeneous graph and denylist are an abstraction of relational database.

The problem as defined poses several challenges. Firstly, the volume of data is huge since graphs contain up to  $10^7$  vertices and  $3 \cdot 10^8$  edges (see Tables V and VI in the Supplementary material for details). Secondly, degree distributions in the Internet tend to follow the *power law* [43]–[45], which means that there are few vertices with a large number of neighbors. As a result, even a local neighborhood of distance one can have a large number of vertices. Thirdly, it is known that malicious activities are localized in the graph [10], [11], forming communities with sharp boundaries. This implies that any successful method for detection of malicious activities should be able to aggregate mainly local information in the graph. In the example in Figure 1 we observe that the two second-level domains with repeated characters (a common

strategy to trick users with small screens) engage with a similar set of vertices in the graph.

In the next section, we describe relevant prior art for this problem in the cybersecurity domain.

### III. RELATED WORK

#### A. Graphical probabilistic models

Graphical probabilistic models capture joint probability distribution of random variables, where each random variable corresponds to a vertex in a graph, and an edge between two vertices signifies a dependence between the corresponding variables. High modeling expressivity comes with a price of exact inference being tractable only for specific subclasses of graphs [46], [47], therefore for practical problems one has to resort to approximate methods [48]–[50]. The most popular inference algorithm is (loopy) belief propagation [51], which iteratively updates states of individual vertices using states of their neighbors from the previous iteration. This approach is an essential component in most following methods [7], [15], [16], [33]–[35]. The general message-passing update can be formulated as:

$$\mathbf{h}_t(v) = r\left(\hat{f}(\mathbf{h}_{t-1}(v)), a\left(\left\{\tilde{f}(\mathbf{h}_{t-1}(u)) \mid \forall u \in \mathcal{N}(v)\right\}\right)\right), \quad (1)$$

where  $\tilde{f}$  first projects representations  $\mathbf{h}_{t-1}$  of vertices  $u \in \mathcal{N}(v)$  (neighborhood of vertex  $v$ ), function  $a$  then aggregates the results, function  $\hat{f}$  projects representation  $\mathbf{h}_{t-1}$  of vertex  $v$ , and finally, function  $r$  operates on a projection of the vertex  $v$  together with the output of the aggregation to create a new representation  $\mathbf{h}_t$ . Concrete algorithms differ in the definition of  $\hat{f}$ ,  $\tilde{f}$ ,  $a$ , and  $r$ .

#### B. Graph Neural Networks

Graph Neural Networks is a family of methods designed for processing graphs with features on vertices or edges. We briefly mention two complementary approaches: Spectral and Spatial, and refer the reader to recent overviews [17], [18] of this rapidly expanding field.

*Spectral* [31], [32] methods embed a graph into the Euclidean space using the graph convolution operator. They can reflect structural dependencies among vertices and their features, but they are restricted to the topologies they were trained on. They are mainly used for reasoning over the whole graph rather than over individual vertices.

*Spatial* approaches leverage spatiality in the graph and define graph convolution based on vertex relations. GraphSAGE [16], one of the first representatives of spatial methods, defines graph convolution as a refined message-passing update using neural networks, running for  $T$  iterations:

$$\mathbf{h}_t(v) = \sigma\left(\mathbf{W}_t\left[\mathbf{h}_{t-1}(v), a_t\left(\left\{\mathbf{h}_{t-1}(u) \mid \forall u \in \mathcal{N}(v)\right\}\right)\right]\right), \quad (2)$$

where  $a_t$  is a parametrized permutation-invariant aggregation function, and  $\mathbf{h}_0(v)$  is initialized to input features  $\mathbf{x}_v$  for each vertex. Note the similarity of the update function (2) to that of

the general message passing algorithm (1). Hence, the spatial GNN can be seen as a general approach to learning the update function.

GNNs were recently used to solve problems in the cybersecurity domain, for example in [19]–[22]. *Heterogeneous* GNNs operate on heterogeneous graphs with various vertex and edge types. To deal with the heterogeneity, many different methods were proposed [33]–[41], all of which are based on the message-passing paradigm.

#### C. Probabilistic Threat Propagation

Probabilistic Threat Propagation (PTP) [7], [15] is a classical graph algorithm from cybersecurity designed for modeling interactions of vertices in the Internet. Given a set of known malicious vertices (denylist) it estimates the *threat*,  $P(v)$ , of each other vertex  $v$  in the graph based on their connections to other vertices. The algorithm defines  $P(v)$  as a solution to a set of linear equations:

$$P(v_i) = \sum_{v_j \in \mathcal{N}(v_i)} w_{ij} P(v_j | v_i = 0), \quad (3)$$

where  $w_{ij}$  are positive edge weights assumed to be normalized to one,  $\sum_j w_{ij} = 1$ . Conditioning  $v_i$  to be benign avoids unwanted direct feedback of a vertex to itself. Since exact solving of (3) requires  $O(n^2)$  time for a graph with  $n$  vertices, the authors propose a message-passing algorithm to find an approximate solution. It initiates  $P_0(v)$  to 1 for vertex from the denylist and 0 otherwise, and updates the solution in  $T$  iterations as

$$P_t(v_i) = \sum_{v_j \in \mathcal{N}(v_i)} w_{ij} (P_{t-1}(v_j) - C_{t-1}(v_i, v_j)), \quad (4)$$

where  $C_{t-1}(v_i, v_j)$  is a portion of  $P_{t-1}(v_j)$  propagated from vertex  $v_i$  in the previous step. In each iteration,  $P_t(v)$  on denylisted vertex is set to 1 again to reinforce the signal. This is a special case of the message passing procedure in Equation (1).

PTP was successfully used to infer malicious second-level domains from a bipartite DNS graph. The most scaled and comprehensive study of PTP is in [52], where it was used for malicious domain discovery. Unlike most of the art, [52] studies how the construction of graph and setting of edge weights affects the accuracy of identification of malicious domains. We, therefore, consider [52] to be state of the art for malicious domain detection and compare it with the proposed method in Section VI.

#### D. Drawbacks for Internet mapping

While the previous approaches achieved success in their domains, they are not sufficiently flexible to model numerous interactions in the Internet.

The main drawback of PTP is that it can propagate only the single scalar variable  $\mathbf{h}_t(v) = P(v)$  and edges can be characterized only by a scalar weight, which limits the description of entities and their interaction. Moreover, PTP does not use any statistical learning to optimize the setting

of the algorithm for a given problem and domain leading to potentially inferior performance [52].

Methods based on GNNs do not suffer from the limitations of PTP as they allow vertices and edges to be characterized by feature vectors. However, a large amount of computation is needed to obtain the result for a single vertex. Because states  $\mathbf{h}_t(v)$  of any vertex  $v$  at any time  $t$  are always the same, the most suitable way to run GNNs is to synchronously compute the results for all vertices at once, enabling effective state reuse. For the type of data encountered in the cybersec domain (the dataset used in this work contains tens of millions of vertices), this makes the inference expensive and training very expensive, especially if results are needed only for a subset of all vertices. The frequent need for retraining only exacerbates this. GNNs have been used on large-scale problems [53], however, speedups were achieved at the expense of expressivity.

To tackle the above problems, the proposed method has the following properties:

- *Local Inference* — the inference is always computed w.r.t. to one individual vertex, which we call a *central vertex* of the inference, taking its local neighborhood as input (this decreases the complexity of the training).
- *Streamlined neighborhood subgraph* — any edge from the neighborhood of a central vertex that does not lie on any shortest path to any vertex in the neighborhood is discarded. The resulting streamlined neighborhood subgraph is processed using the HMILnet architecture [54].
- *State heterogeneity* — the model used for every central vertex is the same (uses the same parameters), however, the internal vertex representations (i.e. the states  $\mathbf{h}_t(v)$ ) are *not* shared, are conditioned on the central vertex, and are thus evaluated for each central vertex individually.

The above-mentioned assumptions allow us to scale the approach to large heterogeneous graphs, which are ubiquitous in computer security and the Internet in general, or even infinite graphs (e.g. streamed data).

#### IV. HMILNET-BASED GRAPH INFERENCE

This section briefly reviews the Multiple Instance Learning (MIL) problem and its hierarchical extension *HMIL*. Then it introduces the *HMILnet* architecture for solving HMIL problems and discusses specifics of HMIL use for homogeneous graph inference, the concepts of *state heterogeneity* and *local inference*, and differences to standard GNNs.

##### A. Multiple Instance Learning

Multiple Instance Learning (MIL) [23], [24] assumes that each sample called *bag*,  $b$ , consists of an arbitrarily large unordered set of vectors  $\{\mathbf{x}_i\}_{i=1}^{|b|}$  called *instances*. Even though it can be assumed that each instance  $\mathbf{x}_i$  is labeled, these labels are not observed, and the main goal is to infer a label only for the whole bag  $b$ . Many different approaches to solving MIL problems have been proposed, and we refer an interested reader to reviews in [25], [26]. Authors of [27]–[29] have independently proposed an approach for solving MIL problems, which uses two multi-layer perceptrons,  $f$ ,  $g$ ,

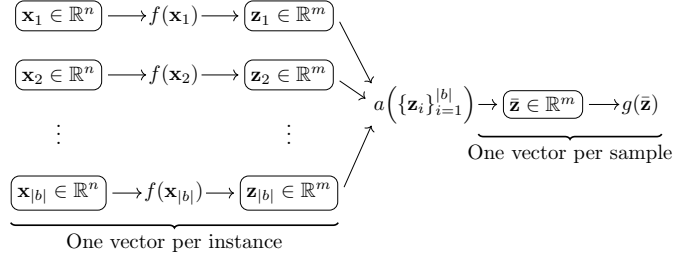


Fig. 2: A depiction of a model to solve MIL problems used in [28], [29].

with an element-wise aggregation function  $a$  sandwiched in between. Specifically, the whole model is defined as follows:

$$g\left(a\left(\left\{f\left(\mathbf{x}_i\right) \mid \mathbf{x}_i \in b\right\}\right)\right). \quad (5)$$

See Figure 2 for a more detailed illustration. If aggregation function  $a$  is differentiable, the whole model is differentiable and therefore optimizable by gradient-based methods. Moreover, [30] generalizes the universal approximation theorem for standard feedforward neural networks to the proposed MIL model.

The two simplest aggregation functions are element-wise mean and max. Although [30] proves that mean aggregation is theoretically sufficient in the MIL framework, [28] discusses that in some situations max can perform better.

##### B. Hierarchical Multiple Instance Learning

Hierarchical Multiple Instance Learning (HMIL) is an intuitive, non-compromising and theoretically justified [30] framework useful for processing hierarchically structured data.

MIL problem is extended in [30] to hierarchical cases, where instances in bags can be bags themselves or Cartesian products of such spaces. Specifically, the class of HMIL samples can be defined recursively as follows:

- *Leafs*: Feature vector  $\mathbf{x} \in \mathbb{R}^n$  is an HMIL sample.
- *Bags*: If instances  $x_1, \dots, x_k$  are HMIL samples following the same *schema* (e.g. all are vectors of the same length or bags of vectors of the same length), then bag  $\{x_i\}_{i=1}^k$  is also an HMIL sample.
- *Tuples*: If  $x_1, \dots, x_l$  are any HMIL samples, then  $(x_1, \dots, x_l)$  is also an HMIL sample.

The extension is important because the class of HMIL samples includes data omnipresent in Internet communication and data exchange such as XMLs or JSONs.

Note that whereas instances in bags are required to be structured identically (follow the same schema), this is not required for tuples.

For a set of HMIL samples following the same schema, a corresponding HMIL model is built by combining three types of layers:

- *Leaf layer*  $f$ : a mapping that accepts a vector  $\mathbf{x}$  from a vector space  $\mathbb{R}^n$  and maps it to  $\mathbb{R}^o$ .
- *Bag layer*  $(a, g)$ : accepts a set of vectors  $b = \{\mathbf{z}_i\}_{i=1}^k$  of the same length  $m$  and processes them as  $g(a(b))$ , where

$a$  is an element-wise aggregation function and  $g: \mathbb{R}^m \mapsto \mathbb{R}^o$  a mapping.

- *Product layer  $r$* : accepts an  $l$ -tuple of arbitrary vectors  $\mathbf{z}_1, \dots, \mathbf{z}_l$ , where  $\mathbf{z}_i \in \mathbb{R}^{m_i}$ , and processes them as  $r([\mathbf{z}_1, \dots, \mathbf{z}_l])$ , where  $r: \mathbb{R}^{\sum_i m_i} \mapsto \mathbb{R}^o$ . Here,  $[\dots]$  denotes concatenation.

The composition is enabled by all three layer types outputting fixed-size vectors.

Bag with instances of an arbitrary (but same) structure are projected to a vector by first projecting each instance with the *same* HMIL (sub)model consisting of appropriate layers to a vector of the same length, and then applying an aggregation function (e.g. mean or max) to obtain one vector representing the whole bag. Equation (5) is an example of a model where a leaf layer  $f$  is followed by a bag layer formed from  $(a, g)$ .

A heterogeneous tuple with items of *different* structure is processed by first projecting each item to a vector with a *different* HMIL (sub)model and then concatenating the results to create a single vector.

The complete model, tailored specifically for each hierarchy of data, is differentiable with respect to its parameters if all its components are. Therefore in application it is recommended to implement  $f$ ,  $g$ , and  $r$  as one or more layers of fully connected neural network layers. Such architecture is called *HMILnet*.

Many applications have missing data, which in the case of HMIL means empty bags, missing items in tuples, and missing values in leaves. In all these cases, empty parts are imputed with learnable parameters, which values are optimized during training in the same way as other model parameters.

HMILnet can be viewed as a feature extractor optimized for given hierarchical data (in the sense of the above definition). Examples of successful applications of the HMIL paradigm in computer security can be found in [27], [54]–[56].

### C. Adapting HMILnet to graph inference

The idea behind the use of HMIL for graph inference is to interpret neighborhood of a fixed (*central*) vertex (provided as *input* to the algorithm) as a *bag*. Both instances in bags and vertices in the neighborhood of a central vertex are unordered and can be arbitrarily large, which justifies the use of HMILnet to learn values about the central vertex [28].

We now describe how the HMIL paradigm is used in the processing of homogeneous graphs, and the extension to heterogeneous graphs is deferred to the next section. After defining several useful terms, we describe HMIL for a neighborhood of a distance one as the simplest case and then proceed to the general definition.

We assume an *undirected homogeneous graph*  $G = (V, E)$  containing a set of *vertices*  $V$  and a set of *edges*  $E$ , where  $E \subseteq \binom{V}{2}$ . We define each edge  $\{u, v\} \in E$  as an *unordered set* of its two endpoints, vertices  $u, v \in V$ . Moreover, we assume that each vertex  $v$  and each edge  $\{u, v\}$  is attributed feature vectors  $\mathbf{x}_v, \mathbf{x}_{v,u}$ , respectively. A *single-step neighborhood* of a single vertex  $v \in V$  is defined as

$$\mathcal{N}(v) = \mathcal{N}_1(v) = \left\{ u \in V \mid \{u, v\} \in E \right\}. \quad (6)$$

A  *$t$ -step neighborhood*  $\mathcal{N}_t(v)$ ,  $t > 1$ , is a generalization defined as the set of vertices whose distance from  $v$  is *exactly*  $t$ . Finally, the set of vertices with a distance at most  $t$  is denoted as  $\mathcal{N}_{\leq t}(v) = \bigcup_{i=0}^t \mathcal{N}_i(v)$ . *Streamlined  $t$ -step neighborhood subgraph* of a vertex  $v$  contains vertices  $\mathcal{N}_{\leq t}(v)$  and only edges lying on one of the shortest paths from  $v$  to any vertex in  $\mathcal{N}_{\leq t}(v)$ .

The inference is then introduced for a vertex  $v$  (called *central vertex*), which is considered fixed. HMIL sample for a single-step neighborhood of a *central vertex*  $v \in V$  is defined as a tuple  $(v, b(v))$ , where  $b(v)$  is a bag containing information from vertices and edges in the neighborhood defined as

$$b(v) = \left\{ \mathbf{z} = [\mathbf{x}_u, \mathbf{x}_{v,u}] \mid u \in \mathcal{N}(v) \right\}, \quad (7)$$

where  $[\cdot, \cdot]$  denotes concatenation. The corresponding HMIL-net model is defined as

$$\mathbf{b}(v) = g \left( a \left( \left\{ \tilde{f}(\mathbf{z}) \mid \mathbf{z} \in b(v) \right\} \right) \right) \quad (8)$$

$$\mathbf{h}(v) = r \left( \left[ \hat{f}(\mathbf{x}_v), \mathbf{b}(v) \right] \right), \quad (9)$$

consisting of two leaf layers  $\hat{f}$  and  $\tilde{f}$ , a bag layer  $(a, g)$ , and a product layer  $r$ .

The model first processes each vertex  $u \in \mathcal{N}(v)$  (an instance in bag  $b(v)$ ) with a leaf layer  $\tilde{f}$ , and then by applying a bag layer  $(a, g)$  we obtain a representation of the bag  $\mathbf{b}(v)$ . In parallel, a representation of the central vertex  $v$  is obtained by applying a leaf layer  $\hat{f}$  on its feature vector  $\mathbf{x}_v$ . Finally, we concatenate the two outputs together using a product layer  $r$ .

When extending the above for processing two-step neighborhoods, the single-step construction is repeated twice, but importantly over the streamlined neighborhood subgraph of the central vertex  $v$ . For each vertex  $u \in \mathcal{N}_1(v)$ , HMIL sample  $(u, b(u))$  is then defined as described above. Since the construction is in the streamlined neighborhood subgraph, the bags  $b(u)$  contain vertices that neighbor  $u$  and are at the distance of two from  $v$  as well as feature vectors corresponding to edges leading to these vertices. Finally, another HMIL sample is produced for a central vertex  $v$ , where feature vectors  $\mathbf{x}_u$  of vertices  $u \in \mathcal{N}(v)$  are replaced with HMIL structures  $b(u)$  created in the previous step. The HMILnet model performing inference is constructed accordingly.

The general algorithm for  $T$ -step HMILnet-based inference on a graph is described in Algorithm 1. Note that no leaf layers  $\tilde{f}_t$  and  $\hat{f}_t$ , bag layers  $(a_t, g_t)$ , or product layers  $r_t$ , in the HMILnet inference model share parameters.

The training of the model follows the standard machine-learning procedure — collecting one or more graphs, extracting some relevant central vertices and their neighborhoods to form a minibatch, deriving labels from the denylist, and updating the whole model w.r.t. some loss.

### D. Differences between HMILnet and GNN

The first distinction between modes of operation of GNNs and HMILnet-based inference is the *state heterogeneity*. GNNs enforce the property that for any vertex  $v$  at any time  $t$ ,  $\mathbf{h}_t(v)$  is

**Algorithm 1**  $T$ -step HMILnet-based inference on a (homogeneous) graph

---

**Input:**  $T$ , graph  $G = (V, E)$ , vertex features  $\mathbf{x}_u$ , edge features  $\mathbf{x}_{u,w}$ , central vertex  $v \in V$ , HMILnet model with layers  $\tilde{f}_t, \hat{f}_t, (a_t, g_t), r_t$  for each  $t = 1, \dots, T$

**Output:**  $\mathbf{h}_T(v)$

```

1:  $\forall u \in V: \mathbf{h}_0(u) = \mathbf{x}_u$ 
2: for  $t = 1$  to  $T$  do
3:   for all  $u \in \mathcal{N}_{T-t}(v)$  do
4:      $\mathbf{b}_t(u) = \left\{ [\mathbf{h}_{t-1}(w), \mathbf{x}_{u,w}] \mid w \in \mathcal{N}(u) \cap \mathcal{N}_{T-t+1}(v) \right\}$ 
5:      $\mathbf{b}_t(u) = g_t \left( a_t \left( \left\{ \tilde{f}_t(\mathbf{z}) \mid \mathbf{z} \in \mathbf{b}_t(u) \right\} \right) \right)$ 
6:      $\mathbf{h}_t(u) = r_t \left( \left[ \hat{f}_t(\mathbf{x}_v), \mathbf{b}_t(u) \right] \right)$ 
7:   end for
8: end for
9: return  $\mathbf{h}_T(v)$ 

```

---

always the same, whereas in HMILnet-based inference  $\mathbf{h}_t(v)$  depends on the current central vertex. This is a consequence of neighborhood streamlining.

Therefore, if enough memory is available, the most efficient way to evaluate GNN is *global inference*—hold all states  $\mathbf{h}_t(v)$  in memory, synchronously compute all states  $\mathbf{h}_{t+1}(v)$  at once, and, having done all  $T$  steps, output final representations  $\mathbf{h}_T(v)$  for all vertices in the graph.

Contrary, HMILnet-based inference uses the *local inference* computational model, where the result  $\mathbf{h}_T(v)$  is computed separately for each vertex  $v$ . The local inference is less computationally efficient when one is interested in inference of a large number of vertices since the computation is not reused. But when one is interested in a small fraction of vertices, as is the case of our application, local inference is more efficient.

Whereas GNNs draw most inspiration from convolutional networks with each layer estimating graph convolution operation, which leads to powerful but hard-to-scale models, the HMILnet-based approach regards the graph (or a collection of graphs) merely as a *database* for querying information about vertices and their relationships. This is beneficial in problems with large graphs and high degrees of vertices, and in particular in computer security by the fact that the maliciousness of the vertex is mainly influenced by its local neighbors with little dependence on the global graph structure.

Because local inference in the HMILnet-based algorithm treats each central vertex as a single training ‘example’, it is more straightforward to construct minibatches for training models and to employ all additional sampling techniques for vertices like stratified sampling or prioritized sampling.

## V. MAPPING THE INTERNET

This section describes concrete application of the above framework to the problem of detection of malicious second-level domains from their interactions in the Internet. However, the proposed algorithm is *general* and it could be employed for processing any other type of network objects. For brevity

from now on, we always refer to ‘second-level domains’ as simply ‘domains’.

We first describe the input and then the construction of *transformed graphs*, which are then used to construct HMIL samples and the corresponding HMILnet model. The remaining part of the section is devoted to implementation aspects.

### A. Input

The method assumes as input an undirected heterogeneous graph similar to the one in Figure 1, with several vertex types corresponding to different network entities like domains, network clients, IP addresses, executables, emails, and others. The interest is on domains, denoting a set of all observed domains  $\mathcal{D}$ , for which a denylist of known malicious domains  $L \subset \mathcal{D}$  is available (considering non-denylisted domains ‘unknown’). The task is to predict whether the remaining domains from  $\mathcal{D} \setminus L$  are malicious or benign.

Vertices of the heterogeneous graph(s) can be partitioned into sets  $\mathcal{D}, \mathcal{V}^{(1)}, \dots, \mathcal{V}^{(C)}$ , where  $\mathcal{D}$  is a set of vertices corresponding to domains and  $\mathcal{V}^{(i)}$  are sets of vertices corresponding to  $C$  network entity types. The transformed graphs described below are constructed from subgraphs  $(\mathcal{G}^{(1)}, \dots, \mathcal{G}^{(C)})$  corresponding to the interaction of domains with one type of network entity. Each subgraph  $\mathcal{G}^{(i)} = (\mathcal{D} \cup \mathcal{V}^{(i)}, \mathcal{E}^{(i)})$ , is *bipartite*—for each edge  $\{d, v\} \in \mathcal{E}^{(i)}$  it holds  $d \in \mathcal{D}$  and  $v \in \mathcal{V}^{(i)}$ .

For instance, one specific  $\mathcal{V}^{(i)}$  can be a set of vertices representing network clients with edge  $\{d, v\} \in \mathcal{E}^{(i)}$  meaning that client  $v \in \mathcal{V}^{(i)}$  communicated with domain  $d \in \mathcal{D}$  during a predefined time window in which the network was observed [7], [52].

In different words, each graph  $\mathcal{G}^{(i)}$  also represents a *homogeneous binary relation* between entities from  $\mathcal{D}$  and  $\mathcal{V}^{(i)}$ .

### B. Transformed graph

To decrease the computational complexity of the inference (and training), graphs  $\mathcal{G}^{(i)} = (\mathcal{D} \cup \mathcal{V}^{(i)}, \mathcal{E}^{(i)})$  are converted to *transformed graphs*  $G^{(i)} = (\mathcal{D}, E^{(i)})$  with only domains  $\mathcal{D}$  as vertices. Vertices corresponding to other network entities are discarded, and edges in the transformed graph exist iff

$$\{d_1, d_2\} \in E^{(i)} \iff \exists v \in \mathcal{V}^{(i)}: \{\{d_1, v\}, \{d_2, v\}\} \subseteq \mathcal{E}^{(i)}, \quad (10)$$

for all different  $d_1, d_2 \in \mathcal{D}$ . In other words, we put edge connecting  $d_1$  and  $d_2$  into a *transformed* graph if and only if there exists a vertex  $v$  that is connected to both in the *original* graph. Figure 3 illustrates the process.

For example, if  $\mathcal{V}^{(i)}$  are network clients, the transformed graph contains an edge between two different domains if and only if there exists a client that communicated with both of them. Therefore, each client creates a clique in the transformed graph containing each contacted domain. For instance, in Figure 1, the big gray vertex representing IP address 23.229.206.69 will connect all eight red vertices representing domains like *technewsup.com* and *beyondgraphicsllc.com* into one clique in the transformed graph of domains.



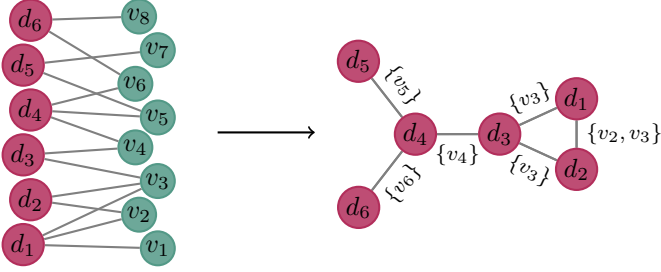


Fig. 3: Graph transformation of a bipartite graph  $\mathcal{G}^{(i)}$  (on the left) to a *transformed graph*  $G^{(i)}$  (on the right). Edges in the transformed graph are labeled with the names of vertices that interacted with both incident vertices in the original graph. Note that vertices  $v_1$ ,  $v_7$ , and  $v_8$  all have only one neighbor and thus do not influence the resulting transformed graph.

As a result, only domains that have at least one interaction in common with another entity in the network, are connected in the transformed graph. Further motivation for this transformation can be found in [52], [57], [58].

### C. Inference

Let's now assume a fixed central vertex  $d \in \mathcal{D}$ , whose neighborhood we want to describe by an HMIL sample, such that the inference can be efficiently performed by an HMILnet model. The HMIL sample is created by first creating the streamlined  $T$ -step neighborhood subgraph of  $d$  in each of the  $C$  transformed graphs, from which  $C$  HMIL (sub)samples  $x_1, \dots, x_C$  are extracted as described in Section IV-C. Thus, each HMIL subsample  $x_i$  describes relations of central vertex  $d$  with one type of entities in its  $T$ -step neighborhood. The final HMIL sample is then constructed as a tuple of HMIL subsamples  $(x_1, \dots, x_C)$ . Finally, an HMILnet model for inference is created to match the sample as described in Section IV (using a product layer stacked on top for processing the tuple). Since the goal is to classify domains into malicious and benign classes, the final layer is of dimension two, corresponding to the predictive probabilities.

A sketch of the whole procedure for one step-neighborhood ( $T = 1$ ) is shown in Figure 4. The pseudocode of the inference is in Algorithm 2.

The described procedure infers a value for a *single* central vertex (single training example), which we regarded as *input* to the Algorithm 2. In the experiments presented in this work, the central vertex corresponds to a single domain. Minibatches during training contains 256 independently sampled samples (each sample corresponds to one central vertex and his neighborhood).

### D. Graph features

In Section IV, it was mentioned that HMILnet model for graph inference can implicitly handle rich features on vertices and edges. Although additional features extracted from individual entities could be added, we have not pursued this idea and extracted features only from raw interaction observations encoded in input graphs  $\mathcal{G}^{(i)}$  (or their transformations  $G^{(i)}$ ).

### Algorithm 2 Heterogeneous mapping of the Internet

**Input:** central vertex (domain)  $d$ , heterogeneous graphs  $(\mathcal{D} \cup \mathcal{V}^{(1)}, \mathcal{E}^{(1)}), \dots, (\mathcal{D} \cup \mathcal{V}^{(C)}, \mathcal{E}^{(C)})$ , HMILnet models for graph inference  $M^{(1)}, \dots, M^{(C)}$ , number of inference steps  $T$ , final product layer  $r$

**Output:** binary classification logits  $\mathbf{o}$

- 1: **for**  $i = 1$  to  $C$  **do** # compute transformed graphs
- $E^{(i)} = \{ \{d_1, d_2\} \mid \{d_1, v\}, \{d_2, v\} \in \mathcal{E}^{(i)},$
- $d_1, d_2 \in \mathcal{D}, v \in \mathcal{V}^{(i)} \}$
- 2:  $G^{(i)} = (\mathcal{D}, E^{(i)})$
- 3: **end for**
- 4: **for**  $i = 1$  to  $C$  **do** # run HMILnet-based inference
- $\mathbf{h}_T^{(i)} = \text{graph-inference}(d, G^{(i)}, M^{(i)}, T)$
- 5: **end for**
- 6:  $\mathbf{o} = r \left( [\mathbf{h}_T^{(1)}, \dots, \mathbf{h}_T^{(C)}] \right)$  # aggregate
- 7: **return**  $\mathbf{o}$

TABLE I: Specification of features used in the experiments. Here,  $\mathcal{G}$  and  $G$  denote (original) bipartite and transformed graphs, and  $\mathcal{N}_{\mathcal{G}}(v)$  and  $\mathcal{N}_G(v)$  neighborhoods of  $v$  in graphs  $\mathcal{G}$  and  $G$ .

name	part of	definition	range
degree	$\mathbf{x}_v$	$ \mathcal{N}_{\mathcal{G}}(v) $	$[1, \infty)$
transformed degree	$\mathbf{x}_v$	$ \mathcal{N}_G(v) $	$[0, \infty)$
neighbor degree	$\mathbf{x}_{v,u}$	$ \mathcal{N}_{\mathcal{G}}(u) $	$[1, \infty)$
intersection	$\mathbf{x}_{v,u}$	$ \mathcal{N}_{\mathcal{G}}(v) \cap \mathcal{N}_{\mathcal{G}}(u) $	$[0, \infty)$
union	$\mathbf{x}_{v,u}$	$ \mathcal{N}_{\mathcal{G}}(v) \cup \mathcal{N}_{\mathcal{G}}(u) $	$[1, \infty)$
Jaccard index	$\mathbf{x}_{v,u}$	$\frac{ \mathcal{N}_{\mathcal{G}}(v) \cap \mathcal{N}_{\mathcal{G}}(u) }{ \mathcal{N}_{\mathcal{G}}(v) \cup \mathcal{N}_{\mathcal{G}}(u) }$	$[0, 1]$
attachment	$\mathbf{x}_{v,u}$	$ \mathcal{N}_{\mathcal{G}}(v)   \mathcal{N}_{\mathcal{G}}(u) $	$[0, \infty)$
detected	$\mathbf{x}_{v,u}$	$u \in L$	$\{0, 1\}$

This is motivated by the fact that in the computer security domain feature extraction tends to be a complicated and time-consuming process. Overall, this decision makes the task harder, as the signal from binary relations tends to be noisy and less discriminative, however, it is less demanding on data collection, processing, and domain knowledge. Finally, this decision enables fair comparison with the PTP algorithm.

By enriching the graph with features extracted from the graph, HMILnet can select informative features or their combination during training. This selection is done manually in [52], where the author searches for optimal construction of graph for PTP algorithm [7]. Table I summarizes all vertex-level  $\mathbf{x}_v$  and edge-level  $\mathbf{x}_{v,u}$  features used in experiments below. The features are a superset of features considered in [52]. Features without an upper bound (e.g. vertex degrees) are mapped by  $x \mapsto \log(x + 1)$  to reduce their dynamic range.

### E. Importance sampling

The power distribution of degrees of vertices found in many graphs representing social networks or the Internet means that there is a small group of domains with extremely large neighborhoods (order of millions). If these domains occur in HMIL samples, bags representing them would have a large number

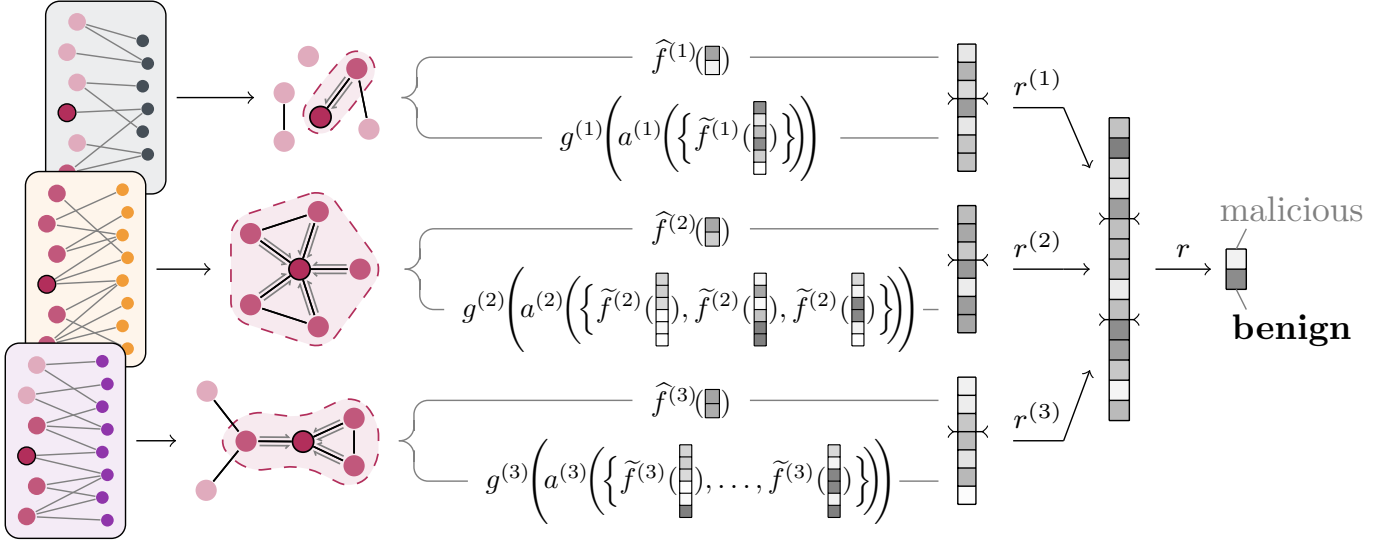


Fig. 4: The whole model procedure for the case when  $T = 1$ . Input bipartite graphs  $\mathcal{G}^{(i)}$  representing input binary relations on the left are first used to obtain the same number of transformed graphs  $G^{(i)}$ . The central vertex representing one particular domain is highlighted in each graph as well as its neighbors in the transformed graph. Note that the left part of each bipartite graph and each transformed graph consist of an identical set of vertices (in our case representing domains) as opposed to edges, which differ with each relation. In the next phase, we aggregate vertex and edge features as explained in Section IV. Each of the three graphs uses (sub)models  $\hat{f}^{(i)}$ ,  $g^{(i)}$ ,  $a^{(i)}$ ,  $\tilde{f}^{(i)}$ ,  $r^{(i)}$  that do not share parameters and may even have different topology. Finally, the product construction is done to obtain the final output, which in the 1-step case is interpreted as a vector of predictive probabilities. Best viewed in color.

of instances (Equation (7)) leading to a high computational complexity of the graph inference part. A solution is to not include the full neighborhood in the bag  $b(v)$ , but only a randomly selected subset, resorting to approximation of the result of aggregation over the bag. Since most domains in the neighborhood are likely ‘unknown’ (non-denylisted) and uniform random sampling would likely miss any informative denylisted malicious domains, we have used importance sampling which selects unknown and known malicious domains with different probabilities.

*Importance sampling* [59], [60] is used to approximate the output of aggregation function  $a$  on bag  $b(v)$  (line 5 in Algorithm 1). Positive (malicious) and negative domains are sampled to a smaller bag with different probabilities (explanation of sampling follows shortly below). Then the mean aggregation function is modified to its *weighted* variant, where the positive and negative instances are weighted by weights  $w^+$  and  $w^-$ , respectively, to ensure the output is an unbiased estimate of the true value.

The weights  $w^+$  and  $w^-$  and sampling probabilities are set as follows. Let  $n^+$  denote the number of positive domains in  $b(v)$  according to the denylist, and  $n^-$  the number of negative (‘unknown’) domains in  $b(v)$ , where  $n^+ \ll n^-$ . To sample a smaller bag  $b'(v)$  from  $b(v)$  we include all  $n^+$  positive domains and  $\min\{n^-, k^-\}$  randomly selected negative domains, where  $k^-$  is a parameter. In the case when  $n^- > k^-$ , ‘unknown’ domains are uniformly sampled without repetition, and each of them is assigned weight  $w^- = n^-/k^-$ . Each positive domain is assigned weight  $w^+ = 1$ .

An additional positive side-effect of the subsampling is an

introduction of stochasticity into learning, which is known to act as a regularizer [61], [62].

## VI. EXPERIMENTAL SETTINGS

In the rest of the text, we describe experimental results. First, we specify how the data were obtained, then various details about implementation and parameter values, and finally, the evaluation protocol. Specific results are then presented in the next Section VII.

### A. Data

Data were kindly provided by *Cisco Systems, Inc.* and consist of several binary relations (represented as a bipartite graph defined in Section V-A) between domains and other network entities. Three following relations were extracted from a subset of anonymized web proxy (W3C) logs processed by Cisco Cognitive Intelligence<sup>1</sup>, and Cisco AMP telemetry<sup>2</sup>:

- *domain-client* — a client has communicated with (issued an HTTP(S) request to) a domain.
- *domain-binary* — a process running a binary file has communicated with a domain.
- *domain-IP* — a domain hostname was resolved to an IP address using DNS.

The data were further enriched with the following three relations extracted from fields in the latest TLS certificate issued to the domain<sup>3</sup>:

<sup>1</sup><https://cognitive.cisco.com>

<sup>2</sup><https://www.cisco.com/c/en/us/products/security/advanced-malware-protection/index.html>

<sup>3</sup>more specifically to one of its possible hostnames



- domain-TLS issuer — a relation connecting domains to the issuer of the TLS certificate. The cardinality type is many-to-one and, therefore, the transformed graph contains a fully connected component for each of the issuers.
- domain-TLS hash — a many-to-one relation connecting a domain to the hash of the TLS certificate. In the transformed graph, domains using the same certificate are connected.
- domain-TLS issue time — domain and the time when the validity period of the certificate starts, stored as a *Unix timestamp*.

Finally, from publicly available information in *WHOIS*, six more relations were extracted: domains and email, nameserver, registrar name, country, WHOIS id, and WHOIS creation time.

Relations domain- $\{\text{client}, \text{binary}, \text{IP}\}$  are of the many-to-many cardinality type—one domain may be connected with an edge to multiple clients/binaries/IPs and vice versa. The remaining cardinalities are of the many-to-one cardinality type.

Graphs of all eleven relations were constructed from data collected during one week-long window. All eleven relations were collected every week. A total of twelve weeks from three months in 2019 were available for experiments — 05-23, 06-03, 06-10, 06-17, 06-24, 06-26, 06-27, 07-01, 07-08, 07-15, 07-22 and 07-29. Further details (specific examples, graph sizes) are available in Tables IV, V, and VI in the Supplementary material. An average bipartite graph describing interaction of domains with a single entity contains around  $7 \cdot 10^6$  vertices and  $3 \cdot 10^8$  edges.

A denylist of malicious domains,  $L$ , provided by Cisco Cognitive Intelligence, tracked 335 malicious campaigns. Each campaign represents a different threat type, its variant, or the stage of the attack. Most of campaigns belong to the family of command and control (for families like ransomware or trojans), represent content delivery or download link of different kinds of malware, or misuse the web advertising via click frauds or other kinds of malvertising. Before each domain was added to the denylist, it was reviewed and categorized by a human analyst.

For each window, we used a snapshot of the denylist available at that time reflecting the knowledge at that time. All weeks of data contained approximately 500 observed denylisted domains. Additional statistics about the denylists are in Table VII in the Supplementary material.

### B. Implementation details

Experimental results presented below were obtained using a one-step ( $T = 1$ ) neighborhood (Figure 4). We expect this to be sufficient in practice since malicious activities tend to be localized [10] and a few-step neighborhood will already cover most of the graph (traversing through vertices of large degrees). We leave the exploration of multi-step versions for future work.

We have compared three different architecture settings differing in the topology of submodel networks implementing

$\hat{f}^{(i)}$ ,  $\tilde{f}^{(i)}$ ,  $g^{(i)}$ , and  $r^{(i)}$  (see Equation (8) and (9)). These four submodel networks have the same topology for each of the eleven input graphs but do not share parameters. Wider  $\mathcal{M}_w$  networks have twice many neurons as the baseline,  $\mathcal{M}_b$ , but keep the number of layers the same. Deeper  $\mathcal{M}_d$  networks have more layers than baseline  $\mathcal{M}_b$ , but a similar number of neurons. Details can be found in Table II. All networks used tanh in layers just before aggregations  $a^{(i)}$  and ReLU otherwise.

Aggregation layers  $a^{(i)}$  implemented concatenation of four element-wise functions: weighted mean, max, parametric *LogSumExp* [63] (a smooth approximation of max):

$$a_{\text{lse}}(\{x_i\}_{i=1}^k; \theta_r) = \frac{1}{\theta_r} \log \left( \frac{1}{k} \sum_{i=1}^k \exp(\theta_r \cdot x_i) \right), \quad (11)$$

and parametric weighted  $p$ -norm [64]:

$$a_{p\text{-norm}}(\{x_i, w_i\}_{i=1}^k; \theta_p, \theta_c) = \left( \frac{\sum_{i=1}^k w_i \cdot |x_i - \theta_c|^{\theta_p}}{\sum_{i=1}^k w_i} \right)^{\frac{1}{\theta_p}}, \quad (12)$$

where  $\theta_r$ ,  $\theta_p$ , and  $\theta_c$  are trainable parameters. The output of the aggregation has four times higher dimension than the input (see Table II).

Because some of the bags may be very large, we employed the sampling procedure described in Section V-E with  $k^- = 100$ . Weighted mean and  $p$ -norm use the resulting importance sampling weights  $w_i$  in the computation. If for a domain some relations are not available at all, or the domain has no neighbors in one or more transformed graphs, the neighborhood reflects in an empty bag treated as described in Section IV-B.

All parameters  $\theta$  of the model therefore are (i) weights and biases used in all feedforward layers, (ii) vectors of default values for cases of missing data or empty neighborhoods in the transformed graph, and (iii) parameter vectors ( $\theta_r$ ,  $\theta_p$  and  $\theta_c$ ) used in aggregation mappings.

Minibatches contained 256 central vertices sampled without repetition containing an equal number of positive and negative examples. One thousand minibatches were created from each graph in one epoch. The training ran for five epochs. Since low false positive rate is paramount in computer security, the loss function was weighted binary cross entropy

$$\mathcal{L}(\theta) = -\frac{1}{n} \sum_{i=1}^n \left( \omega_1 y_i \log p(\hat{y}_i = 1; \theta) + \omega_0 (1 - y_i) \log p(\hat{y}_i = 0; \theta) \right), \quad (13)$$

where  $n$  is the size of the minibatch,  $y_i \in \{0, 1\}$  is  $i$ -th domain binary label,  $p(\hat{y}_i; \theta)$  the probability of predicted label, and  $\omega_0, \omega_1$  are constant weights. All experiments used  $\omega_1 = 0.1$  and  $\omega_0 = 0.9$ , Adam optimizer [65] with the default parameters, Glorot normal initialization [66] for weights, and zero initialization for biases.

Experiments were run at an Amazon EC2 instance with 36 CPU cores and 72GiB of RAM.

TABLE II: Numbers of neurons in model architectures  $\mathcal{M}_b$ ,  $\mathcal{M}_w$  and  $\mathcal{M}_d$ . Each number in tuples represents one feedforward layer with the given number of neurons. The length of the tuple specifies the number of layers in the submodel. For example, the baseline architecture  $\mathcal{M}_b$  implements leaf layer  $\hat{f}^{(i)}$  as a sequence of three dense layers with 2, 10, and 10 neurons.

(sub)model	$\hat{f}^{(i)}$	$\tilde{f}^{(i)}$	$g^{(i)}$	$r^{(i)}$	$r$
$\mathcal{M}_b$	(2, 10, 10)	(6, 30, 30)	(120, 60, 60)	(70, 20)	(220, 100, 2)
$\mathcal{M}_w$	(2, 20)	(6, 60)	(240, 120)	(140, 20)	(1320, 2)
$\mathcal{M}_d$	(2, 5, 5, 5)	(6, 15, 15, 15, 15)	(60, 60, 30, 30)	(35, 20, 20)	(220, 60, 60, 2)

### C. Evaluation

The data (time windows) were split into train/validation/test sets as follows: weeks 06–10, 06–27 and 07–22 were used for testing; week 06–24 for validation, and all others for training. Hyperparameters were selected on the validation week to prevent overfitting.

The key component of the validation is the denylist which has two roles in the methodology: i) it is used to compute features (Table I) for model prediction, and ii) it is used as a source of labels for evaluation of the prediction accuracy. Thus, it is essential that the evaluation protocol prevents leaking of the labels to the features and, consequently, to predictions. In the feature-generating role, the denylist is assumed to be incomplete, implying training the model under the positive-unlabeled scenario. In the accuracy evaluation role, the denylist is assumed to be complete, domains on the list are considered malicious, and domains missing from the list are considered benign.

These specifics are well known in the community, with available evaluation protocols [7], [52], which we follow for comparison with the prior art. Specifically, the model is trained on all available training data, but the denylist corresponding to the validation set is split randomly into  $K$  disjoint folds. The evaluation runs for each fold independently as follows: i) domains from the active fold are removed from the denylist (thus considered ‘unknown’), and the features are computed only from denylists of the remaining folds; ii) domains from the active fold and all benign domains are predicted by the model using the features. After processing all  $K$  folds, we have one prediction for all malicious samples and  $K$  predictions for the unknown samples. The final prediction of benign samples is obtained by aggregation using the max operator to simulate the worst-case scenario with respect to false-positive rate.

A potential drawback of using any evaluation that splits data into training and testing parts is that the validated domain can be present in the training set with the correct label, hence the learning system could have ‘memorized’ it. We argue that this is highly unlikely since the used features are in the form of statistics (Table I). This conjecture is experimentally validated using a sensitivity study (the Grill test) in Section VII-D.

## VII. EXPERIMENTAL RESULTS

Experiments are presented in four blocks. First, we show results when modeling domain relationship with a single entity, which is needed for comparison to the prior art (PTP). Then, we present experiments when all entities are used, highlighting the advantage of the proposed algorithm, since PTP is not

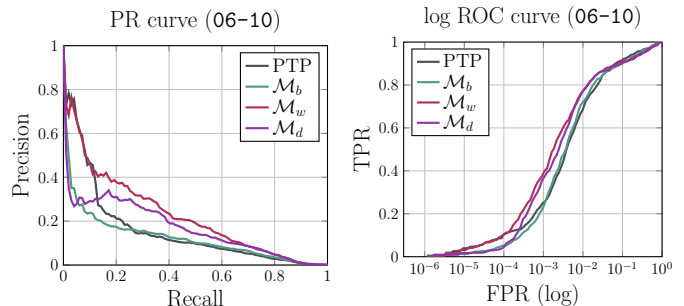


Fig. 5: A PR curve and an ROC curve with logarithmic  $x$  axis comparing the performance of the three proposed architectures to the PTP algorithm. In these experiments, only one relation is employed.

applicable. Following ablation studies investigate sensitivity to the size of the training set and sensitivity to the noise in ground-truth labels.

Experimental results are presented as a precision-recall (PR) curve and a receiver operating characteristic (ROC) curve with logarithmically scaled  $x$ -axis to emphasize behavior on low false positive rate. Average Precision (AP) and Area Under the ROC Curve (AUC) scalar metrics are used in Table III for summary. The main text contains results computed from one testing week (06–10), the rest is available in the Supplementary material.

### A. Single relation (PTP comparison)

Probabilistic Threat Propagation (PTP) is compared to our algorithm on data sourced from a bipartite graph capturing *domain-client* relations (recall that PTP cannot model multiple relations). The implementation of PTP was taken from [52] and used 20 iterations. From PR and ROC curves shown in Figure 5 we see that both algorithms perform the same for very low false positive rates (below 0.0001) or low recall (below 0.15), but for higher false positive rates and recall the proposed algorithm performs better. The results in the remaining weeks from the testing set look similar and can be found in Supplementary material A. The same graphs also show that wider networks  $\mathcal{M}_w$  are better than the deeper network and the baseline.

### B. All relations

Next, Figure 6 (and Table III) shows the PR and ROC curves when the proposed method uses all eleven relations. For the sake of comparison, PTP is shown, but keep in mind that

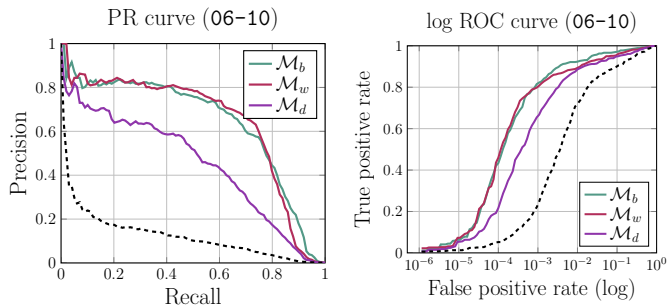


Fig. 6: A PR curve and an ROC curve with logarithmic  $x$  axis comparing the performance of the three proposed architectures when all eleven relations are used. The black dashed curve corresponds to the baseline ( $\mathcal{M}_b$ ) performance when only the domain-client relation is used.

PTP can use only the *domain-client* graph due to its inherent limitations. Adding additional relationships to the proposed model improves their performance approximately three times according to average precision. Contrary to the above experiments, where the wider architecture  $\mathcal{M}_w$  was clearly the best, here it performs similarly to baseline architecture  $\mathcal{M}_b$ . Deeper architecture  $\mathcal{M}_d$  with a smaller number of neurons was inferior. Results on the remaining weeks in the testing set are in Supplementary material B.

#### C. Size of the training set

The dependence of the proposed method on the size of the training set was studied by comparing models training on graphs from the first 1, 3, 5, or 8 weeks (8 weeks means the full training set). The training of all experiments used the same number of training steps (minibatches), potentially reusing data more frequently if needed. The used experimental settings also allows the study of concept drift, since small training sets used the oldest training set. The model used the baseline architecture  $\mathcal{M}_b$  with all eleven relations.

Experimental results are summarised in Table III. Surprisingly, there is a relatively small dependence (1 – 2 percent) on the size of the training set. This is probably because the network traffic observed during different weeks is highly correlated, and the concept drift present in the data is not significant enough to alter the performance. Experimental results on the remaining weeks are in Supplementary material C.

#### D. Grill test

To assess that the model does not overfit to specific domains seen during training, we used a technique from [67], further called *Grill test*. During the Grill test, we first sample a subset of denylisted domains proportionally to the size of each malware family, omit them from the sampled domains during training (they are never a central vertex), and if they appear in the neighborhood of other domains, they are considered ‘unknown’. This way, the model cannot memorize them as malware examples. During evaluation, only sampled domains are used as ground truth for positive labels. This tests the model on domains that have never been seen before and appear

TABLE III: Values of the AP and the AUC metrics for the three testing weeks. Each subtable represents a different experiment—*single relation (comparison to PTP)*, *all relations, less training data*, and the *Grill test*. The greatest score in each experiment and column is marked in bold. Note that the fifth and eleventh rows correspond to the identical settings, but are included for easier comparison.

		06-10		06-27		07-22	
		AP	AUC	AP	AUC	AP	AUC
single rel.	PTP	0.152	<b>0.962</b>	0.120	0.958	0.142	0.954
	$\mathcal{M}_b$	0.119	0.958	0.152	0.959	0.154	0.955
	$\mathcal{M}_w$	<b>0.221</b>	0.956	<b>0.237</b>	0.966	<b>0.220</b>	0.957
	$\mathcal{M}_d$	0.163	0.956	0.189	<b>0.967</b>	0.202	<b>0.958</b>
all rel.	$\mathcal{M}_b$	0.637	<b>0.988</b>	<b>0.687</b>	<b>0.990</b>	<b>0.657</b>	<b>0.988</b>
	$\mathcal{M}_w$	<b>0.638</b>	0.984	0.678	0.982	0.654	0.980
	$\mathcal{M}_d$	0.445	0.978	0.498	0.983	0.468	0.980
less data	1	<b>0.688</b>	0.974	0.696	0.980	0.665	0.975
	3	0.678	0.983	<b>0.698</b>	0.984	<b>0.670</b>	0.981
	5	0.633	0.976	0.671	0.984	0.631	0.977
	8 (all)	0.637	<b>0.988</b>	0.687	<b>0.990</b>	0.657	<b>0.988</b>
GT	$\mathcal{M}_b$	0.445	0.951	0.468	0.966	0.468	0.959

during the testing first time. Moreover, adding this noise to labels simulates incomplete denylist during training, which surely happens in practice. Again a baseline architecture  $\mathcal{M}_b$  is used for simplicity.

According to the results shown in Table III, there is a 3% drop in performance according to the AUC, which might be partially due to the noise but also due to the smaller number of positive samples in the training set. AP has decreased by 30%, which we attribute to the fact that the PR curve is sensitive to class priors, which have changed. From these results we conclude that the proposed method performs well on previously unseen malicious domains. Additional details can be found in Supplementary material D.

#### E. Practical discussion

The main aim of this work is to present a *general* approach for malicious activity detection from interactions, which is not exclusive to only observing second-level domains. In a similar fashion, IP addresses, binary files, emails, or other network entities, could be used instead. As a result, even more possible attack surfaces would be monitored.

Since the cybersecurity landscape is rapidly evolving, HMILnet-based inference like most other methods leveraging statistical machine learning requires regular retraining. However, this is not difficult to perform—the method requires only “raw” bipartite graphs and updated denylist as input, no external features potentially hard or expensive to obtain. Moreover, our technique relies mostly on the behavior of the domains and not any other more specific features, which mitigates the need for frequent retraining.

The specific application of the proposed technique on second-level domain detection shares fundamental drawbacks and benefits with other detection engines that rely on domain

reputation. For example, otherwise legitimate domains are sometimes exploited for malicious activity. Domains suddenly acting maliciously would be detected by the method, as it is based on observing behavior directly. When the owner recovers the domain and it stops showing signs of malicious activity, the method will soon stop detecting it. The same reasoning could be for instance applied to fast-flux evasion techniques. In a graph that reflects domains' behavior, the properties of the immediate neighborhood of individual instances of a single fast-fluxed domain would be very similar. To avoid the detection, attackers would have to switch between individual instances frequently enough, or completely change the behavior from instance to instance. This increases attack costs and significantly lowers the appeal of such type of attack.

### VIII. CONCLUSION AND FUTURE WORK

This work demonstrated how the Hierarchical Multiple Instance Learning paradigm can be used to perform local inference in a streamlined neighborhood subgraph and compared it to the existing approaches. The HMILnet-based inference scales well to huge graphs with variable vertex degrees, and due to the state heterogeneity property, it is possible to run inference on small subsets of vertices and the method is trivially parallelizable. We show that HMILnet-based inference also performs well on the malicious domain discovery problem when only plain binary relations between entities in the network are employed. Our proposed method outperforms the state-of-the-art PTP algorithm when a PTP-compatible subset of data is used, however, the performance increases even more when all available data are used. Moreover, we demonstrate that the method produces a classifier that generalizes beyond simple memoization of known threats.

In comparison to the prior art PTP algorithm, where each edge can be described by, at most, a single scalar weight and the best choice is application-dependent, the proposed scheme handles rich hierarchical features on both vertices and edges. We consider attributing external features to vertices or edges an interesting future research direction as it will likely improve performance at the cost of increased computational complexity.

One more area that remains to be explored is to manually analyze some of the detected second-level domains and model behavior on them and then provide human-understandable interpretations for model decisions.

### REFERENCES

- [1] Š. Mandlák, T. Pevný, V. Šmídl, and L. Bajer, "Malicious internet entity detection using local graph inference," *IEEE Transactions on Information Forensics and Security*, vol. 19, pp. 3554–3566, 2024.
- [2] K. Bartos, M. Sofka, and V. Franc, "Optimized invariant representation of network traffic for detecting unseen malware variants," in *25th USENIX Security Symposium (USENIX Security 16)*, (Austin, TX), pp. 807–822, USENIX Association, Aug. 2016.
- [3] J. Zhang, P. A. Porras, and J. Ullrich, "Highly predictive blacklisting," *login Usenix Mag.*, vol. 33, no. 6, 2008.
- [4] M. Antonakakis, R. Perdisci, D. Dagon, W. Lee, and N. Feamster, "Building a dynamic reputation system for dns," in *USENIX Security Symposium*, 2010.
- [5] L. Bilge, E. Kirda, C. Kruegel, and M. Balduzzi, "EXPOSURE: finding malicious domains using passive DNS analysis," in *Proceedings of the Network and Distributed System Security Symposium, NDSS 2011, San Diego, California, USA, 6th February - 9th February 2011*, The Internet Society, 2011.
- [6] F. Pendlebury, F. Pierazzi, R. Jordaney, J. Kinder, and L. Cavallaro, "TESSERACT: eliminating experimental bias in malware classification across space and time," *CoRR*, vol. abs/1807.07838, 2018.
- [7] K. M. Carter, N. Idika, and W. W. Streilein, "Probabilistic threat propagation for network security," *IEEE Trans. Inf. Forensics Secur.*, vol. 9, no. 9, pp. 1394–1405, 2014.
- [8] B. Coskun, S. Dietrich, and N. Memon, "Friends of an enemy: identifying local members of peer-to-peer botnets using mutual contacts," in *Proceedings of the 26th Annual Computer Security Applications Conference*, pp. 131–140, 2010.
- [9] S. Philips, M. Yee, E. Kao, and C. Anderson, "Detecting activity-based communities using dynamic membership propagation," in *2012 IEEE International Conference on Acoustics, Speech and Signal Processing (ICASSP)*, pp. 2085–2088, IEEE, 2012.
- [10] T. Yu, R. Lippmann, J. Riordan, and S. Boyer, "EMBER: A global perspective on extreme malicious behavior," in *ACM Int. Conf. Proceeding Ser.*, pp. 1–12, 2010.
- [11] M. P. Collins, T. J. Shimeall, S. Faber, J. Janies, R. Weaver, M. De Shon, and J. Kadane, "Using uncleanliness to predict future botnet addresses," in *Proceedings of the 7th ACM SIGCOMM conference on Internet measurement*, pp. 93–104, 2007.
- [12] A. Oprea, Z. Li, T. Yen, S. H. Chin, and S. A. Alrwais, "Detection of early-stage enterprise infection by mining large-scale log data," in *45th Annual IEEE/IFIP International Conference on Dependable Systems and Networks, DSN 2015, Rio de Janeiro, Brazil, June 22-25, 2015*, pp. 45–56, IEEE Computer Society, 2015.
- [13] M. Rezvani, V. Sekulic, A. Ignjatovic, E. Bertino, and S. Jha, "Interdependent security risk analysis of hosts and flows," *IEEE Transactions on Information Forensics and Security*, vol. 10, no. 11, pp. 2325–2339, 2015.
- [14] A. Ahuja, H. Gandhi, R. Shorey, D. Kulkarni, and J. Tew, "Plumewalk: Towards threat provenance localization for iot networks," in *2019 11th International Conference on Communication Systems Networks (COMSNETS)*, pp. 383–390, 2019.
- [15] K. M. Carter, N. Idika, and W. W. Streilein, "Probabilistic threat propagation for malicious activity detection," in *ICASSP, IEEE Int. Conf. Acoust. Speech Signal Process. - Proc.*, pp. 2940–2944, oct 2013.
- [16] W. L. Hamilton, Z. Ying, and J. Leskovec, "Inductive representation learning on large graphs," in *Advances in Neural Information Processing Systems 30: Annual Conference on Neural Information Processing Systems 2017, December 4-9, 2017, Long Beach, CA, USA* (I. Guyon, U. von Luxburg, S. Bengio, H. M. Wallach, R. Fergus, S. V. N. Vishwanathan, and R. Garnett, eds.), pp. 1024–1034, 2017.
- [17] J. Zhou, G. Cui, Z. Zhang, C. Yang, Z. Liu, and M. Sun, "Graph neural networks: A review of methods and applications," *CoRR*, vol. abs/1812.08434, 2018.
- [18] Z. Wu, S. Pan, F. Chen, G. Long, C. Zhang, and P. S. Yu, "A comprehensive survey on graph neural networks," *CoRR*, vol. abs/1901.00596, 2019.
- [19] J. Busch, A. Kocheturov, V. Tresp, and T. Seidl, "NF-GNN: network flow graph neural networks for malware detection and classification," in *SSDBM 2021: 33rd International Conference on Scientific and Statistical Database Management, Tampa, FL, USA, July 6-7, 2021* (Q. Zhu, X. Zhu, Y. Tu, Z. Xu, and A. Kumar, eds.), pp. 121–132, ACM, 2021.
- [20] J. D. Herath, P. P. Wakodikar, P. Yang, and G. Yan, "Cfgeplainer: Explaining graph neural network-based malware classification from control flow graphs," in *52nd Annual IEEE/IFIP International Conference on Dependable Systems and Networks, DSN 2022, Baltimore, MD, USA, June 27-30, 2022*, pp. 172–184, IEEE, 2022.
- [21] W. Wei, M. Qiao, E. Butler, and D. Jadav, "Graph representation learning based vulnerable target identification in ransomware attacks," in *IEEE International Conference on Big Data, Big Data 2022, Osaka, Japan, December 17-20, 2022* (S. Tsumoto, Y. Ohsawa, L. Chen, D. V. den Poel, X. Hu, Y. Motomura, T. Takagi, L. Wu, Y. Xie, A. Abe, and V. Raghavan, eds.), pp. 2423–2430, IEEE, 2022.
- [22] H. Zhu and J. Lu, "Graph-based intrusion detection system using general behavior learning," in *IEEE Global Communications Conference, GLOBECOM 2022, Rio de Janeiro, Brazil, December 4-8, 2022*, pp. 2621–2626, IEEE, 2022.
- [23] T. G. Dietterich, R. H. Lathrop, and T. Lozano-Pérez, "Solving the multiple instance problem with axis-parallel rectangles," *Artif. Intell.*, vol. 89, no. 1-2, pp. 31–71, 1997.

- [24] O. Maron and T. Lozano-Pérez, “A Framework for Multiple-Instance Learning,” in *Adv. Neural Inf. Process. Syst. 10* (M. I. Jordan, M. J. Kearns, and S. A. Solla, eds.), pp. 570–576, MIT Press, 1998.
- [25] J. Amores, “Multiple instance classification: Review, taxonomy and comparative study,” 2013.
- [26] J. Foulds and E. Frank, “A review of multi-instance learning assumptions,” mar 2010.
- [27] T. Pevný and P. Somol, “Discriminative models for multi-instance problems with tree structure,” in *AISeC 2016 - Proc. 2016 ACM Work. Artif. Intell. Secur. co-located with CCS 2016*, 2016.
- [28] T. Pevný and P. Somol, “Using neural network formalism to solve multiple-instance problems,” *Lect. Notes Comput. Sci. (including Subser. Lect. Notes Artif. Intell. Lect. Notes Bioinformatics)*, vol. 10261 LNCS, no. Mil, pp. 135–142, 2017.
- [29] H. Edwards and A. J. Storkey, “Towards a neural statistician,” *CoRR*, vol. abs/1606.02185, 2016.
- [30] T. Pevný and V. Kovarik, “Approximation capability of neural networks on spaces of probability measures and tree-structured domains,” *CoRR*, vol. abs/1906.00764, 2019.
- [31] M. M. Bronstein, J. Bruna, Y. LeCun, A. Szlam, and P. Vandergheynst, “Geometric deep learning: going beyond euclidean data,” *CoRR*, vol. abs/1611.08097, 2016.
- [32] T. N. Kipf and M. Welling, “Semi-supervised classification with graph convolutional networks,” *CoRR*, vol. abs/1609.02907, 2016.
- [33] S. Chang, W. Han, J. Tang, G. Qi, C. C. Aggarwal, and T. S. Huang, “Heterogeneous network embedding via deep architectures,” in *Proceedings of the 21th ACM SIGKDD International Conference on Knowledge Discovery and Data Mining, Sydney, NSW, Australia, August 10-13, 2015* (L. Cao, C. Zhang, T. Joachims, G. I. Webb, D. D. Margineantu, and G. Williams, eds.), pp. 119–128, ACM, 2015.
- [34] H. Gui, J. Liu, F. Tao, M. Jiang, B. Norick, and J. Han, “Large-scale embedding learning in heterogeneous event data,” in *IEEE 16th International Conference on Data Mining, ICDM 2016, December 12-15, 2016, Barcelona, Spain* (F. Bonchi, J. Domingo-Ferrer, R. Baeza-Yates, Z. Zhou, and X. Wu, eds.), pp. 907–912, IEEE Computer Society, 2016.
- [35] T. Fu, W. Lee, and Z. Lei, “Hin2vec: Explore meta-paths in heterogeneous information networks for representation learning,” in *Proceedings of the 2017 ACM Conference on Information and Knowledge Management, CIKM 2017, Singapore, November 06 - 10, 2017* (E. Lim, M. Winslett, M. Sanderson, A. W. Fu, J. Sun, J. S. Culpepper, E. Lo, J. C. Ho, D. Donato, R. Agrawal, Y. Zheng, C. Castillo, A. Sun, V. S. Tseng, and C. Li, eds.), pp. 1797–1806, ACM, 2017.
- [36] C. Shi, B. Hu, W. X. Zhao, and P. S. Yu, “Heterogeneous information network embedding for recommendation,” *CoRR*, vol. abs/1711.10730, 2017.
- [37] Y. Dong, N. V. Chawla, and A. Swami, “metapath2vec: Scalable representation learning for heterogeneous networks,” in *Proceedings of the 23rd ACM SIGKDD International Conference on Knowledge Discovery and Data Mining, Halifax, NS, Canada, August 13 - 17, 2017*, pp. 135–144, ACM, 2017.
- [38] Y. Zhang, Y. Xiong, X. Kong, S. Li, J. Mi, and Y. Zhu, “Deep collective classification in heterogeneous information networks,” in *Proceedings of the 2018 World Wide Web Conference on World Wide Web, WWW 2018, Lyon, France, April 23-27, 2018* (P. Champin, F. Gandon, M. Lalmas, and P. G. Ipeirotis, eds.), pp. 399–408, ACM, 2018.
- [39] L. Sun, L. He, Z. Huang, B. Cao, C. Xia, X. Wei, and P. S. Yu, “Joint embedding of meta-path and meta-graph for heterogeneous information networks,” *CoRR*, vol. abs/1809.04110, 2018.
- [40] S. Fan, J. Zhu, X. Han, C. Shi, L. Hu, B. Ma, and Y. Li, “Metapath-guided heterogeneous graph neural network for intent recommendation,” in *Proceedings of the 25th ACM SIGKDD International Conference on Knowledge Discovery & Data Mining, KDD 2019, Anchorage, AK, USA, August 4-8, 2019* (A. Teredesai, V. Kumar, Y. Li, R. Rosales, E. Terzi, and G. Karypis, eds.), pp. 2478–2486, ACM, 2019.
- [41] X. Wang, H. Ji, C. Shi, B. Wang, P. Cui, P. S. Yu, and Y. Ye, “Heterogeneous graph attention network,” *CoRR*, vol. abs/1903.07293, 2019.
- [42] G. Blanchard, G. Lee, and C. Scott, “Semi-supervised novelty detection,” *J. Mach. Learn. Res.*, vol. 11, pp. 2973–3009, 2010.
- [43] L. Adamic, B. Huberman, A.-L. Barabasi, R. Albert, H. Jeong, and G. Bianconi, “Power-law distribution of the world wide web,” *Science*, vol. 287, pp. 2115–, 03 2000.
- [44] G. Siganos, M. Faloutsos, P. Faloutsos, and C. Faloutsos, “Power laws and the as-level internet topology,” *Networking, IEEE/ACM Transactions on*, vol. 11, pp. 514 – 524, 09 2003.
- [45] M. Faloutsos, P. Faloutsos, and C. Faloutsos, “On power-law relationships of the internet topology,” *ACM SIGCOMM Computer Communication Review*, vol. 29, 03 2003.
- [46] L. E. Baum and T. Petrie, “Statistical Inference for Probabilistic Functions of Finite State Markov Chains,” *Ann. Math. Stat.*, vol. 37, pp. 1554–1563, dec 1966.
- [47] J. Pearl, *Probabilistic Reasoning in Intelligent Systems*. Elsevier, 1988.
- [48] B. J. Frey and D. J. C. MacKay, “A revolution: Belief propagation in graphs with cycles,” in *Advances in Neural Information Processing Systems 10, [NIPS Conference, Denver, Colorado, USA, 1997]* (M. I. Jordan, M. J. Kearns, and S. A. Solla, eds.), pp. 479–485, The MIT Press, 1997.
- [49] L. Wang, J. Liu, and S. Z. Li, “MRF parameter estimation by MCMC method,” *Pattern Recognit.*, vol. 33, no. 11, pp. 1919–1925, 2000.
- [50] P. Kohli and P. H. Torr, “Efficiently solving dynamic markov random fields using graph cuts,” in *Proc. IEEE Int. Conf. Comput. Vis.*, vol. II, pp. 922–929, 2005.
- [51] F. R. Kschischang, B. J. Frey, and H. A. Loeliger, “Factor graphs and the sum-product algorithm,” *IEEE Trans. Inf. Theory*, vol. 47, no. 2, pp. 498–519, 2001.
- [52] J. Jusko, *Graph-Based Detection of Malicious Network Communities*. PhD thesis, Czech Technical University, 2017. AAI29119838.
- [53] E. Rossi, F. Frasca, B. Chamberlain, D. Eynard, M. M. Bronstein, and F. Monti, “SIGN: scalable inception graph neural networks,” *CoRR*, vol. abs/2004.11198, 2020.
- [54] Šimon Mandlík, M. Račinský, V. Lisý, and T. Pevný, “Jsongrinder.jl: automated differentiable neural architecture for embedding arbitrary json data,” *Journal of Machine Learning Research*, vol. 23, no. 298, pp. 1–5, 2022.
- [55] T. Pevný and M. Dedic, “Nested multiple instance learning in modelling of HTTP network traffic,” *CoRR*, vol. abs/2002.04059, 2020.
- [56] S. Mandlik and T. Pevny, “Mapping the internet: Modelling entity interactions in complex heterogeneous networks,” 2021.
- [57] L. Liu, S. Saha, R. Torres, J. Xu, P. N. Tan, A. Nucci, and M. Mellia, “Detecting malicious clients in ISP networks using HTTP connectivity graph and flow information,” in *ASONAM 2014 - Proc. 2014 IEEE/ACM Int. Conf. Adv. Soc. Networks Anal. Min.*, pp. 150–157, Institute of Electrical and Electronics Engineers Inc., oct 2014.
- [58] P. K. Manadhata, S. Yadav, P. Rao, and W. G. Horne, “Detecting malicious domains via graph inference,” in *Computer Security - ESORICS 2014 - 19th European Symposium on Research in Computer Security, Wrocław, Poland, September 7-11, 2014. Proceedings, Part I* (M. Kutylowski and J. Vaidya, eds.), vol. 8712 of *Lecture Notes in Computer Science*, pp. 1–18, Springer, 2014.
- [59] A. B. Owen, *Monte Carlo theory, methods and examples*. 2013.
- [60] H. Kahn and M. A. W., “Methods of reducing sample size in monte carlo computations,” *Journal of the Operations Research Society of America*, vol. 1, no. 5, 1953.
- [61] N. Srivastava, G. Hinton, A. Krizhevsky, I. Sutskever, and R. Salakhutdinov, “Dropout: A simple way to prevent neural networks from overfitting,” *Journal of Machine Learning Research*, vol. 15, no. 56, pp. 1929–1958, 2014.
- [62] S. Ioffe and C. Szegedy, “Batch normalization: Accelerating deep network training by reducing internal covariate shift,” *CoRR*, vol. abs/1502.03167, 2015.
- [63] O. Z. Kraus, L. J. Ba, and B. J. Frey, “Classifying and segmenting microscopy images using convolutional multiple instance learning,” *CoRR*, vol. abs/1511.05286, 2015.
- [64] C. Gulcehre, K. Cho, R. Pascanu, and Y. Bengio, “Learned-Norm Pooling for Deep Feedforward and Recurrent Neural Networks,” in *Mach. Learn. Knowl. Discov. Databases* (T. Calders, F. Esposito, E. Hüllermeier, and R. Meo, eds.), (Berlin, Heidelberg), pp. 530–546, Springer Berlin Heidelberg, 2014.
- [65] D. P. Kingma and J. Ba, “Adam: A method for stochastic optimization,” in *3rd International Conference on Learning Representations, ICLR 2015, San Diego, CA, USA, May 7-9, 2015, Conference Track Proceedings* (Y. Bengio and Y. LeCun, eds.), 2015.
- [66] X. Glorot and Y. Bengio, “Understanding the difficulty of training deep feedforward neural networks,” in *Proceedings of the Thirteenth International Conference on Artificial Intelligence and Statistics, AISTATS 2010, Chia Laguna Resort, Sardinia, Italy, May 13-15, 2010* (Y. W. Teh and D. M. Titterton, eds.), vol. 9 of *JMLR Proceedings*, pp. 249–256, JMLR.org, 2010.
- [67] M. Grill and T. Pevný, “Learning combination of anomaly detectors for security domain,” *Comput. Networks*, vol. 107, pp. 55–63, 2016.

SUPPLEMENTARY MATERIAL A  
RESULTS: SINGLE RELATION

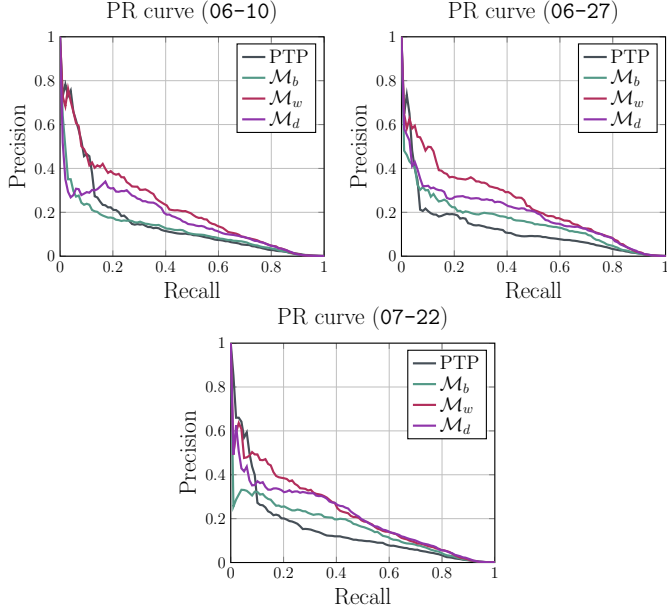


Fig. 7: PR curves comparing the performance of the three proposed architectures (baseline  $\mathcal{M}_b$ , wider  $\mathcal{M}_w$ , and deeper  $\mathcal{M}_d$ ) to the PTP algorithm. Three figures are plotted, each corresponding to one of the testing datasets.

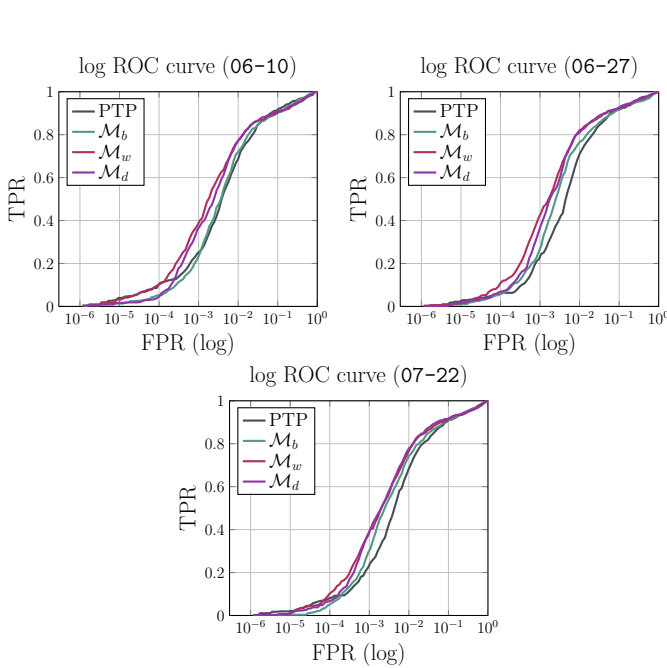


Fig. 8: ROC curves comparing the performance of the three proposed architectures (baseline  $\mathcal{M}_b$ , wider  $\mathcal{M}_w$ , and deeper  $\mathcal{M}_d$ ) to the PTP algorithm. Three figures are plotted, each corresponding to one of the training datasets. The logarithmic scale is used for  $x$ -axis.

SUPPLEMENTARY MATERIAL B  
RESULTS: ALL RELATIONS

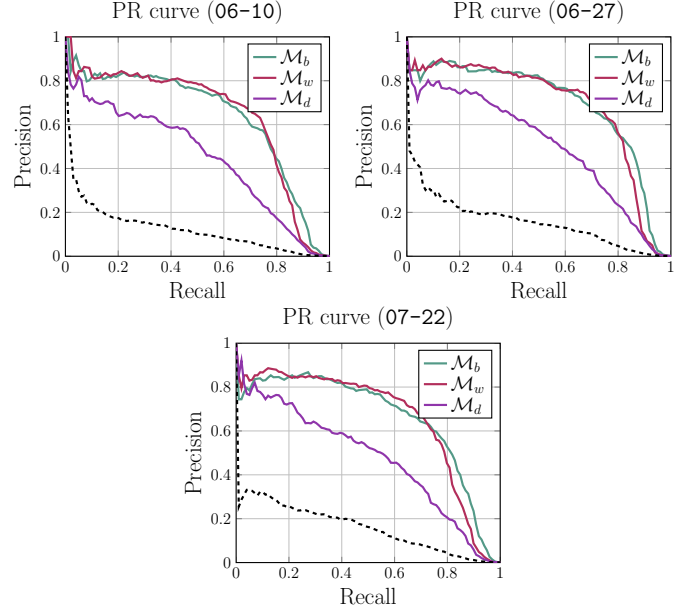


Fig. 9: PR curves comparing the performance of three proposed architectures (baseline  $\mathcal{M}_b$ , wider  $\mathcal{M}_w$ , and deeper  $\mathcal{M}_d$ ) when all eleven relations are used. Three figures are plotted, each corresponding to one of the testing datasets. The black dashed curve corresponds to the baseline ( $\mathcal{M}_b$ ) performance when only the domain-client relation is used.

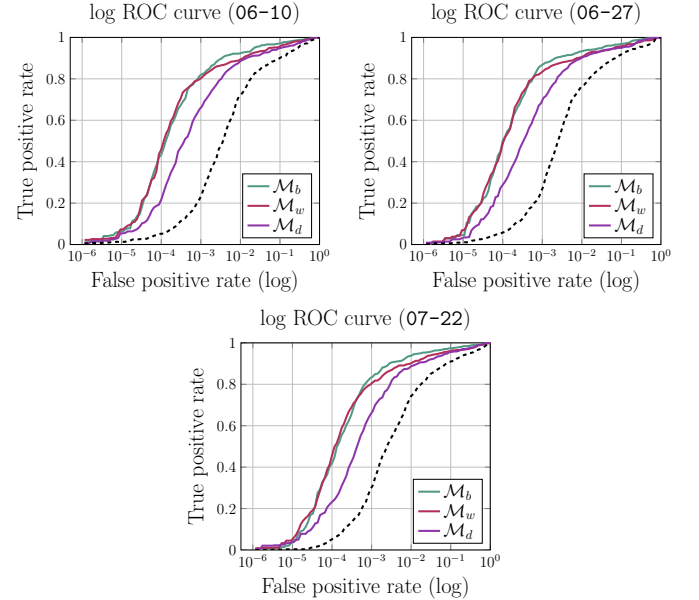


Fig. 10: ROC curves comparing the performance of three proposed architectures (baseline  $\mathcal{M}_b$ , wider  $\mathcal{M}_w$ , and deeper  $\mathcal{M}_d$ ) when all eleven relations are used. Three figures are plotted, each corresponding to one of the training datasets. The logarithmic scale is used for  $x$ -axis. The black dashed curve corresponds to the baseline ( $\mathcal{M}_b$ ) performance when only the domain-client relation is used.



**SUPPLEMENTARY MATERIAL C**  
**RESULTS: SIZE OF THE TRAINING SET**

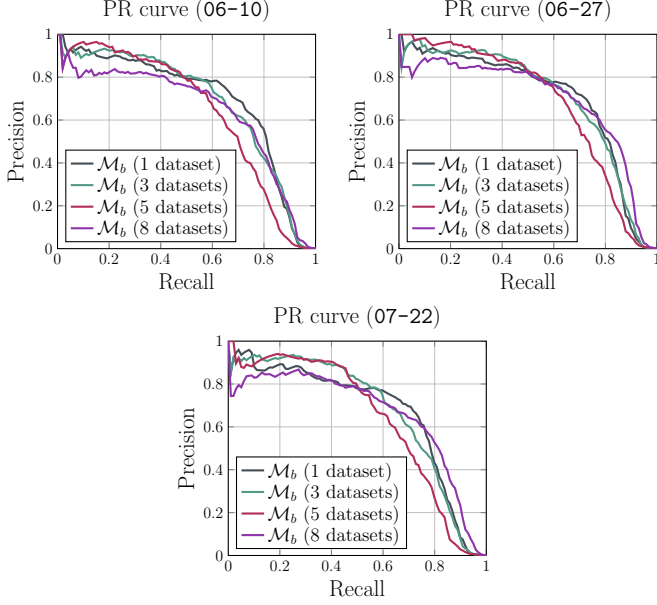


Fig. 11: PR curves comparing the performance of the baseline architecture  $\mathcal{M}_b$  when a different number of datasets is used for training. Three figures are plotted, each corresponding to one of the testing datasets.

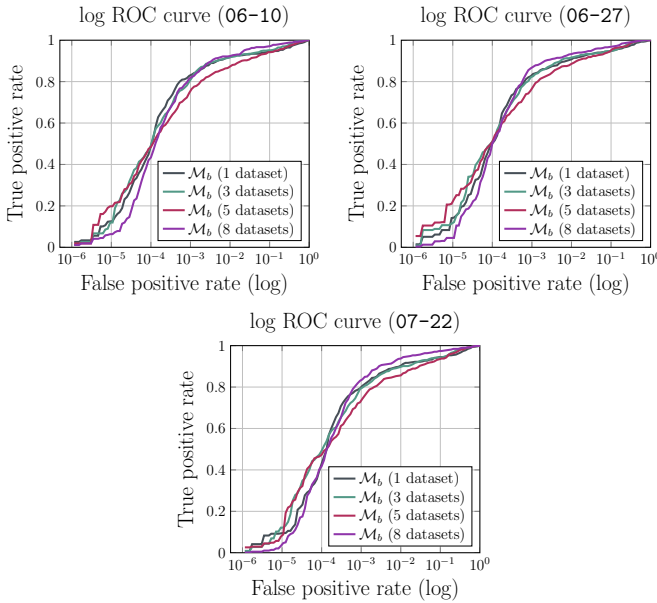


Fig. 12: ROC curves comparing the performance of the baseline architecture  $\mathcal{M}_b$  when a different number of datasets is used for training. Three figures are plotted, each corresponding to one of the training datasets. The logarithmic scale is used for  $x$ -axis.

**SUPPLEMENTARY MATERIAL D**  
**RESULTS: GRILL TEST**

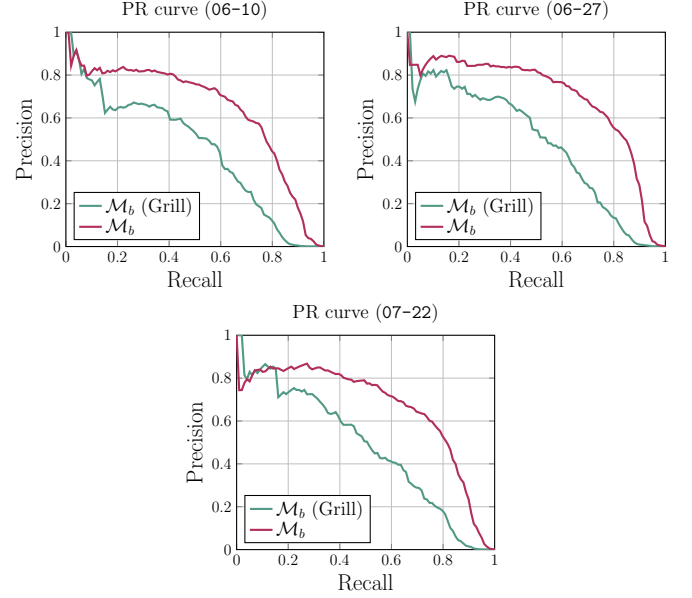


Fig. 13: PR curves comparing the performance of the baseline architecture  $\mathcal{M}_b$  when the Grill test is (not) used. Three figures are plotted, each corresponding to one of the training datasets.

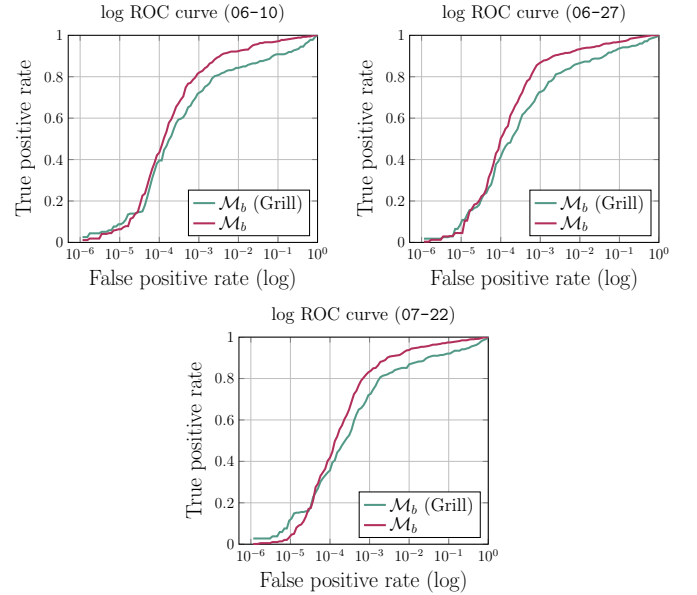


Fig. 14: ROC curves comparing the performance of the baseline architecture  $\mathcal{M}_b$  when the Grill test is (not) used. Three figures are plotted, each corresponding to one of the training datasets. The logarithmic scale is used for  $x$ -axis.

SUPPLEMENTARY MATERIAL E  
DATA DETAILS

TABLE IV: All relations used in our experiments, with their cardinality type and several examples of specific relation pairs (edges in a bipartite graph). Each edge is specified as  $(u; v)$  to avoid confusion as commas may be used in  $u$  or  $v$ . M2M stands for ‘many-to-many’ and M2O for ‘many-to-one’ cardinality type. Longer names are shortened using ellipsis (...).

name (domain-*)	card. type	examples
*-client	M2M	(tottenhamhotspur.com; S8g) (loanstreet.com.my; 2Pu3) (healthlabtesting.com; 2WLu)
*-binary	M2M	(kotonoha-jiten.com; 15CBF8...) (wonderslim.com; B41781...) (pythonprogramming.net; CF6ACB...)
*-IP address	M2M	(quickpayportal.com; 208.78.141.18) (jobwinner.ch; 217.71.91.48) (tottenhamhotspur.com; 104.16.54.111)
*-TLS issuer	M2O	(cratejoy.com; CN=Amazon, OU=Server CA 1B, O=Amazon, C=US) (creative-serving.com; CN=COMODO RSA Domain Validation Secure Server...) (healthlabtesting.com; CN=Symantec Class 3 Secure Server CA...)
*-TLS hash	M2O	(timeoutdubai.com; 90c093...) (boomerang.com; e577e6...) (quickpayportal.com; 85bdd8...)
*-TLS issue time	M2O	(jobwinner.ch; 1496041693) (healthlabtesting.com; 1445558400) (flatmates.com.au; 1502150400)
*-WHOIS email	M2O	(unstableunicorns.com; unstableunicorns.com@*sbyproxy.com) (albertlee.biz; abuse@godaddy.com) (crownplazalondonthecity.com; crownplazalondonthecity.com@*sbyproxy.com )
*-WHOIS nameserver	M2O	(grd779.com; ns2.hover.com) (celeritascdn.com; lady.ns.cloudflare.com) (smresources.org; ns-495.awsdns-61.com)
*-WHOIS registrar name	M2O	(unblocked.how; eNom, Inc.) (rev-stripe.com; Amazon Registrar, Inc.) (chisaintjosephhealth.org; Register.com, Inc.)
*-WHOIS country	M2O	(thefriscostl.com; CANADA) (getwsone.com; UNITED STATES) (notify.support; PANAMA)
*-WHOIS registrar id	M2O	(lo3trk.com; 468) (watchcrichd.org; 472) (bozsh.com; 1479)
*-WHOIS timestamp	M2O	(unblocked.how; 15293) (comicplanet.net; 15159) (unpublishedflight.com; 15553)

TABLE V: Numbers of vertices of each type in each dataset.

date	domain	client	binary	IP	TLS hash	TLS issuer	TLS issue time	WHOIS email	WHOIS name-server	WHOIS registrar name	WHOIS country	WHOIS registrar id	WHOIS time-stamp
05-23	710 167	3 419 758	245 999	2 357 441	6 217	374 531	160 343	18 537	15 972	1 111	160	959	901
06-03	631 828	3 151 105	232 507	2 247 940	5 631	337 558	142 944	16 442	14 803	989	157	849	901
06-10	644 868	3 140 231	236 052	2 268 276	5 745	348 298	148 844	16 834	14 913	969	160	833	904
06-17	630 532	3 114 985	242 696	2 305 323	5 618	340 934	145 032	16 808	14 973	945	161	806	904
06-26	648 960	3 175 500	238 535	2 316 943	5 732	350 155	149 609	17 519	15 454	954	160	805	902
06-27	616 958	3 106 120	240 931	2 256 445	5 484	334 996	142 453	16 468	14 942	909	158	763	901
07-01	613 601	3 055 840	240 909	2 277 775	5 433	332 991	141 471	16 373	14 866	894	157	743	897
07-08	557 253	2 894 017	224 571	2 117 016	5 077	307 541	129 249	14 319	13 756	810	160	665	890
07-15	608 327	2 943 900	241 631	2 222 769	5 504	330 853	140 718	16 168	14 834	861	158	717	899
07-22	600 814	2 929 311	239 520	2 193 113	5 423	326 592	138 604	16 214	14 764	842	156	693	898
07-29	588 039	2 873 682	237 436	2 162 197	5 194	320 663	135 980	15 785	14 475	806	150	656	898

TABLE VI: Numbers of edges between domains and other types of vertices in each dataset.

date	client	binary	IP	TLS hash	TLS issuer	TLS issue time	WHOIS email	WHOIS name-server	WHOIS registrar name	WHOIS country	WHOIS registrar id	WHOIS time-stamp
05-23	334 320 003	4 073 050	9 314 998	465 879	465 879	465 879	44 613	122 231	42 804	39 506	46 589	46 603
06-03	292 659 940	3 639 635	8 356 254	419 035	419 035	419 035	38 974	108 077	37 349	34 538	40 690	40 704
06-10	299 532 603	3 785 134	8 902 097	430 878	430 878	430 878	39 766	110 423	38 213	35 321	41 543	41 555
06-17	293 466 696	3 813 715	8 803 587	420 926	420 926	420 926	39 322	109 466	37 741	34 906	41 072	41 088
06-26	306 114 224	3 846 992	9 141 868	431 772	431 772	431 772	41 035	114 242	39 370	36 328	42 832	42 845
06-27	291 065 433	3 821 056	8 740 732	412 836	412 836	412 836	38 296	107 202	36 775	33 943	39 996	40 009
07-01	285 920 746	3 789 277	8 649 546	410 419	410 419	410 419	37 797	106 055	36 256	33 520	39 480	39 494
07-08	251 616 117	3 361 849	7 917 765	376 934	376 934	376 934	33 028	936 23	317 36	292 40	345 25	345 34
07-15	278 227 235	3 693 630	8 869 060	406 339	406 339	406 339	37 536	105 356	36 008	33 288	39 180	39 193
07-22	278 975 786	3 765 391	8 627 468	400 566	400 566	400 566	37 407	104 908	35 844	33 015	39 017	39 031
07-29	274 507 944	3 701 055	8 475 127	392 479	392 479	392 479	36 473	102 514	35 002	32 228	38 021	38 034

TABLE VII: Numbers of malicious domains in each of the datasets. In the first row, there is the number of domains that are both in the denylist and in the observed dataset, and in the second row, we give the ratio of the number of denylisted domains to the total number of domains in the dataset.

	05-23	06-03	06-10	06-17	06-24	06-26	06-27	07-01	07-08	07-15	07-22	07-29
$ L \cap \mathcal{D} $	656	578	535	557	538	557	552	555	512	557	577	548
$ L \cap \mathcal{D} / \mathcal{D} $	0.924%	0.915%	0.830%	0.883%	0.865%	0.858%	0.895%	0.904%	0.919%	0.916%	0.960%	0.932%